Model of low-pass filtering of local field potentials in brain tissue

C. Bédard,[1] H. Kröger,[1,*] and A. Destexhe[2]
[1]*Département de Physique, Université Laval, Québec, Québec G1K 7P4, Canada*
[2]*Unité de Neurosciences Intégratives et Computationnelles, CNRS, 1 Avenue de la Terrasse, 91198 Gif-sur-Yvette, France*
(Received 27 June 2005; revised manuscript received 13 January 2006; published 19 May 2006)

Local field potentials (LFPs) are routinely measured experimentally in brain tissue, and exhibit strong low-pass frequency filtering properties, with high frequencies (such as action potentials) being visible only at very short distances (≈ 10 μm) from the recording electrode. Understanding this filtering is crucial to relate LFP signals with neuronal activity, but not much is known about the exact mechanisms underlying this low-pass filtering. In this paper, we investigate a possible biophysical mechanism for the low-pass filtering properties of LFPs. We investigate the propagation of electric fields and its frequency dependence close to the current source, i.e., at length scales in the order of average interneuronal distances. We take into account the presence of a high density of cellular membranes around current sources, such as glial cells. By considering them as passive cells, we show that under the influence of the electric source field, they respond by polarization. Because of the finite velocity of ionic charge movements, this polarization will not be instantaneous. Consequently, the induced electric field will be frequency-dependent, and much reduced for high frequencies. Our model establishes that this situation is analogous to an equivalent RC circuit, or better yet a system of coupled RC circuits. We present a number of numerical simulations of an induced electric field for biologically realistic values of parameters, and show the frequency filtering effect as well as the attenuation of extracellular potentials with distance. We suggest that induced electric fields in passive cells surrounding neurons are the physical origin of frequency filtering properties of LFPs. Experimentally testable predictions are provided allowing us to verify the validity of this model.

DOI: 10.1103/PhysRevE.73.051911 PACS number(s): 87.19.La, 87.17.Aa

I. INTRODUCTION

Electric fields of the brain, which are experimentally observable either on the surface of the scalp, or by microelectrodes, are due to currents in dendrites and the soma of cortical pyramidal cells [1,2]. Experimental measurements of electric fields created in the brain distinguish three scenarios: (i) Local field potentials (LFPs) denote the electric potential recorded locally in the immediate neighborhood of neurons using microelectrodes of a size comparable to the cell body. (ii) The electrocorticogram (ECoG) refers to measurements of the field using electrodes of a diameter of the size of about 1 mm, placed on the cortical surface. (iii) The electroencephalogram (EEG) is measured at the surface of the scalp using electrodes of a centimeter scale. In the latter case, the electric potential is recorded after conduction through cerobrospinal fluid, cranium, and scalp, and corresponds to the situation where the source of the electric signals in the cortex is located far from the site of detection on the scalp (at a scale $\lambda \approx 10^3 d_{nn}$, where $d_{nn}=0.027$ mm is the average distance between cortical neurons).

By contrast with the intracellular or membrane potential, which biophysical properties have been extensively studied [3–5], the mechanisms underlying the genesis of LFPs are still unclear. LFP recordings routinely show strong high-frequency attenuation properties, because action potentials are only visible for a few neurons immediately adjacent to the electrode, while low-frequency components result from large populations of neurons in the local network. Using LFPs, it has been shown that low-frequency oscillations (0–4 Hz) have a large scale coherence, while the coherence of higher frequency (20–60 Hz) oscillations is short ranged. In anesthetized animals, it was shown that oscillations of up to 4 Hz have a coherence range in the order of several millimeters, while oscillations of 20–60 Hz have a coherence of a submillimeter range [6,7]. The local coherence of high-frequency oscillations was also shown in the visual system of anesthetized cats, where gamma oscillations (30–50 Hz) appear only within restricted cortical areas and time windows [8,9]. The same difference of coherence between low- and high-frequency oscillations was also demonstrated in nonanesthetized animals, respectively, during sleep in a state of low-frequency waves and waking [10]. Similar findings have been reported for human EEG [11].

A full understanding of the mechanisms underlying the genesis of EEG and LFP signals is required to relate these signals with neuronal activity. Several models of EEG or LFP activity have been proposed previously (e.g., see [1,12–17]). These models always considered current sources embedded in a homogeneous extracellular fluid. In such homogeneous media, however, there cannot be any frequency filtering property. Extracellular space consists of a complex folding of intermixed layers of fluids and membranes, while the extracellular fluid represents only a few percent of the available space [19,20]. Due to the complex nature of this medium, it is very difficult to draw theories or to model LFPs properly, and one needs to make approximations. In a previous paper [18], we considered current sources with various continuous profiles of conductivity according to a spherical symmetry, and showed that it can lead to a low-pass

*Corresponding author. Electronic address: hkroger@phy.ulaval.ca

 ©2006 The American Physical Society

frequency filtering. This showed that strong inhomogeneities in conductivity and permittivity in extracellular space can lead to a low-pass frequency filtering, but this approach was not satisfactory because high-pass filters could also be obtained, in contradiction to experiments. In addition, this model predicted frequency attenuation which was not quantitative, as action potentials were still visible at the 1 mm distance, which is in contrast to what is observed experimentally.

In the present paper, we go one step further and consider an explicit structure of extracellular space, in which we study the interaction of the electric field with the membranes surrounding neurons. Neurons are surrounded by densely packed membranes of other neurons and glial cells [19–21], a situation which we approximate here by considering a series of passive spherical membranes around the source, all embedded in a conducting fluid. We show that the low-pass frequency filtering can be determined by the membranes of such passive cells and the phenomenon of electric polarization.

II. GENERAL THEORY

In this section, we describe the theoretical framework of the model. We start by outlining the model (Sec. II A), where a simplified structure of extracellular space is considered. We also describe its main simplifications and assumptions. Next, we discuss the physical implementation of this model (Sec. II B), while the propagation of the electric fields will be analyzed more formally in the next sections (Secs. II C–II F).

A. Model of extracellular space

In Ref. [18], we considered a model where the electrical properties of extracellular space are described by two parameters only: conductivity σ and permittivity ϵ. Both σ and ϵ were considered to vary with location according to some *ad hoc* assumptions. V_ω, the frequency ω component of the electric potential V obtained by a Fourier transformation of the potential as a function of time, was shown to obey the equation

$$\Delta V_\omega + (\vec{\nabla} V_\omega) \cdot \left(\frac{\vec{\nabla}(\sigma + i\omega\epsilon)}{(\sigma + i\omega\epsilon)} \right) = 0. \quad (1)$$

The physical behavior of the solution is essentially determined by the expression $1 + i\omega\epsilon/\sigma$. When a strong inhomogeneity occurs, one may have $\omega\epsilon/\sigma \gg 1$. This means that a strong phase difference may exist between the electric current and potential, i.e., a large impedance. In a neurophysiological context, such behavior is likely to occur at the interface between the extracellular fluid (high conductivity) and the membranes of cells (low conductivity). This situation was considered previously in the context of a simplified representation of extracellular space, in which the inhomogeneities of conductivity were assumed to be of spherical symmetry around the source [18]. Moreover, the equation above assumes that the charge density of the extracellular medium is zero when its potential is zero, which is not entirely true since there is an excess of positive charges on the exterior surface of neuronal membranes at rest.

In the present work, we consider an explicit structure of extracellular space in order to more realistically account for these inhomogeneities of conductivity. The extracellular space is assumed to be composed of active cells producing current sources (neurons), and passive cells (glia), all embedded in a conducting fluid. Neurons are characterized by various voltage-dependent and synaptic ion channels, and they will be considered here as the sole source of the electric field in extracellular space. On the other hand, glial cells are very densely packed in interneuronal space, sometimes surrounding the soma or the dendrites of neurons [20,21]. Glial cells normally do not have dominant voltage-dependent channel activity, and they rather play a role in maintaining extracellular ionic concentrations. Like neurons, they have an excess of negative charges inside the cell, which is responsible for a negative resting potential (for most central neurons, this resting membrane potential is around -60 to -80 mV). They will be considered here as "passive" and representative of all non-neuronal cell types characterized by a resting membrane potential. We will show that such passive cells can be polarized by the electric field produced by neurons. This polarization has an inertia and a characteristic relaxation time which may have important consequences to the properties of propagation of local field potentials. These different cell types are separated by extracellular fluid, which plays the role of a conducting medium, i.e., allows for the flow of electric currents. In the remainder of this text, we will use the term passive cell to represent the various cell types around neurons, but also bearing in mind that they may represent other neurons as well.

Another simplification is that we will consider these passive cells as of elementary shapes (spherical or cubic). Under such a simplification, it will be possible to treat the propagation of field potentials analytically and design simulations using standard numeric tools. Our primary objective here is to explore one essential physical principle underlying the frequency-filtering properties of extracellular space, based on the polarization of passive membranes surrounding neuronal sources. We assume that such a principle will be valid regardless of the morphological complexity and spatial arrangement of neurons and other cell types in extracellular space. As a consequence of these simplifications, the present work does not attempt to provide a quantitative description but rather an exploration of first principles that could be applied in a later work to the actual complexity of biological tissue.

The arrangement of charges in our model is schematized in Fig. 1(a), where we delimited 5 regions. The membrane of the passive cell (region 3) separates the intracellular fluid (region 5) from the extracellular fluid (region 1), both of which are electrically neutral. The negative charges in excess in the intracellular medium agglutinate in the region immediately adjacent to the membrane (region 4), while the analogous region at the exterior surface of the membrane (region 2) contains the positive ions in excess in the extracellular space. This arrangement results in a charge distribution [schematized in Fig. 1(b)] which creates a strong electric field inside the membrane and a membrane potential.

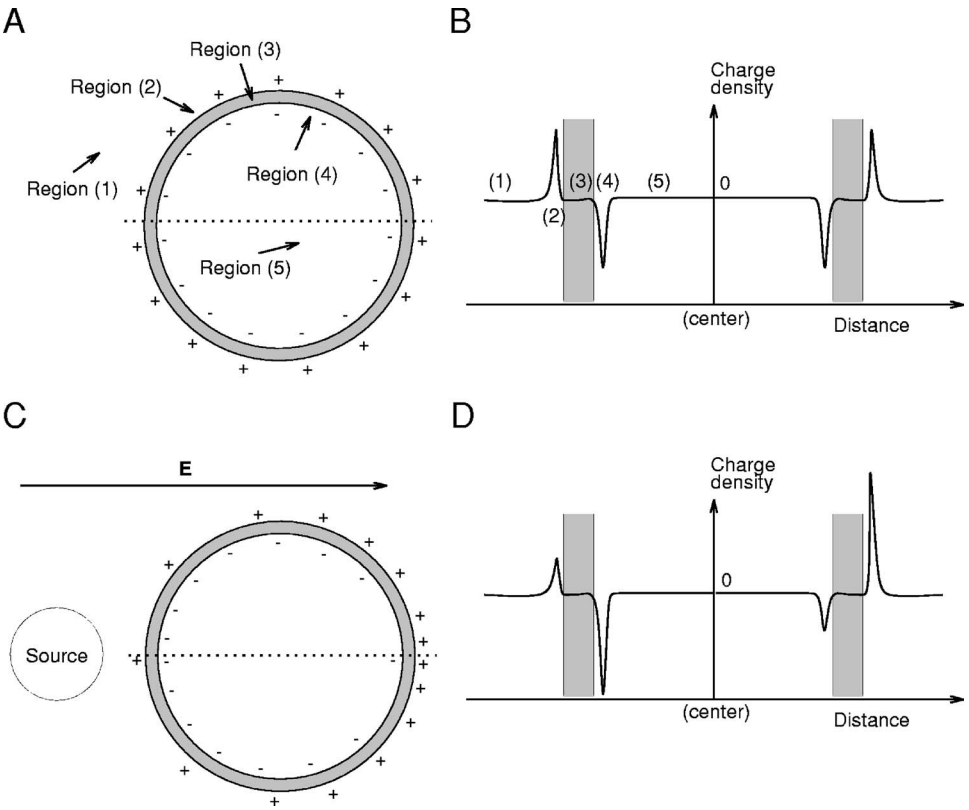

FIG. 1. Scheme of charge distribution around the membrane of a passive cell. (a) Charge distribution at rest. The following regions are defined: the extracellular fluid (region 1), the region immediately adjacent to the exterior of the membrane where positive charges are concentrated (region 2), the membrane (region 3, in gray), the region immediately adjacent to the interior of the membrane where negative charges are concentrated (region 4), and the intracellular (cytoplasmic) fluid (region 5). (b) Schematic representation of the charge density as a function of distance [along the horizontal dotted line in (a)]. (c) Redistribution of charges in the presence of an electric field. The ions move away from or towards the source, according to their charge, resulting in a polarization of the cell. (d) Schematic representation of the charge density predicted from (c).

The behavior of such a system depends on the values of conductivity and permittivity in these different regions (they are considered constant within each region). The extracellular fluid (region 1) has good electric conductance properties. We have taken as conductivity $\sigma_1=4\ \Omega^{-1}\ \mathrm{m}^{-1}$, consistent with biological data $\sigma=3.3-5\ \Omega^{-1}\ \mathrm{m}^{-1}$, taken from measurements of a specific impedance of the rabbit cerebral cortex [22]. This value is comparable to the conductivity of salt water ($\sigma_{sw}=2.5\ \Omega^{-1}\ \mathrm{m}^{-1}$). The permittivity is given by $\epsilon_1=70\ \epsilon_0$, corresponding to salt water. Here $\epsilon_0=8.854\times10^{-12}$ Farad/m denotes the permittivity of the vacuum. In region 2, to the best of our knowledge, there are no experimental data on conductivity close to the membrane. We have chosen the values of $\sigma_2=0.7\times10^{-7}\ \Omega^{-1}\ \mathrm{m}^{-1}$ and $\epsilon_2=1.1\times10^{-10}$ Farad $\mathrm{m}^{-1}\approx12\epsilon_0$ for region 2. Such a choice is not inconsistent with biological observations. First, electron microscopic photographs taken from the region near the membrane reflect very little light, which hints to quite a low conductivity compared to the conductivity of region 1. We consider it as plausible that permittivity in region 2 should be smaller than in region 1. Our choice of σ_2 and ϵ_2 corresponds to a Maxwell time T_M yielding a cutoff frequency $f_c\approx100$ Hz, which was also the choice given in a previous study investigating composite materials [23].

For passive cells, we neglect ion channels and pumps located in the membrane, which is equivalent in assuming the absence of any electric current across the membrane. Therefore, region 3 has zero conductivity perpendicular to the membrane surface. The capacity of a cellular membrane has been measured and is about $C=10^{-2}$ Farad/m^2 [4]. Approximating the membrane by a parallel plate capacitor (with surface S and distance d, obeying $C=\epsilon S/d$), one estimates the electric permittivity of membrane to $\epsilon_3=10^{-10}$ Farad/m. Hence we used the parameters $\sigma_3=0$, and $\epsilon_3=12\epsilon_0$.

Thus the basic idea behind the model is as follows: As represented in Fig. 1, we consider a single spherical passive cell under the influence of an electric field. The electric field will induce a polarization of the cell by reorganizing its charge distribution [Figs. 1(c) and 1(d)]. This polarization will create a secondary electric field, with field lines connecting those opposite charges. It is a customary notation to call the original electric field the *source field*, or the *primary field*, while the field due to polarization is called the *induced field*, or the *secondary field*. The physical electric field is the sum (in the sense of vectors) of both, the source and the induced field. This induced field will be highly dependent on frequency, for high frequencies, the "inertia" of the charge movement in regions 2 and 4 will limit such a polarization, and will reduce the effect of the induced field. This phenomenon is the basis of the model of frequency-dependent local field potentials presented in this paper.

B. Physical implementation of the model

We introduce here the toolbox of physics used for the construction of our model, in which we consider neurons as the principal sources of the electric current. In electrodynamics, one distinguishes between a current source and a potential source. A current source, e.g., in an electric circuit, means that if the electric current is used to do some work, the source maintains its level of current. Likewise, a potential source maintains its electric potential. Although neurons are generally considered as current sources, here we have chosen to consider them as potential sources, for the following rea-

sons. First, these two types of sources are equivalent for calculating extracellular potentials. The electric potential within a given region D depends on the limit conditions at the border of this region, and not on the type of source (current vs potential source). Second, it is much easier to calculate the potential using limit conditions on the potential (Dirichlet conditions) than using limit conditions with currents (Neumann conditions). Third, potentials are better constrained from experiments and their range of values is better known than currents (for example, the amplitude of membrane potential variations in neurons is of the order of 10–20 mV for subthreshold activity, and of about 100 mV during spikes).

Let us suppose that we are given a source of electric field, representing a neuron with some open ion channels. The motion of ions through those channels gives a current density, and also creates a distribution of charges (ions). According to the Maxwell equations, a given distribution of currents and charges (plus information on the polarization and induction properties of the medium) determines the magnetic field, the electric field, and hence the electric potential. In a first step, we consider the effect of the electric field on a single passive cell.

The source electric field is the origin of two physical phenomena. First, the electric field exerts a force on charged particles (ions) and thus creates a motion of charge carriers, i.e., an electric current. Second, the electric field creates a displacement of charges in the borderline region of the membrane of the passive cell (region 2). This displacement creates an induced potential due to polarization. However, this polarization is not instantaneous, due to the "inertia" of charge movements. The charges on the membrane move relatively slowly, which will be responsible for a slow time dependence of the polarization, before reaching equilibrium. The characteristic time scale of such a process is given by Maxwell's relaxation time T_M [see Eq. (7) below], which depends on the properties of the medium, such as resistivity and permittivity. The temporal behavior of the source is dynamic, which can be characterized by some characteristic time scale T_S. For example, during the creation of an action potential, ion channels open and ionic currents flow, and the electric field and the potential changes. After a certain time the neuron source goes back to its state of rest. This means that the electric current will vanish after some delay. For example, in a typical neuron, the width of the action potential is typically of the order of 2 m s. The polarization and relaxation dynamics of the passive cell depends on both time scales, T_S and T_M. This situation holds in the case of an ideal dielectric medium (conductivity zero, for example, pure water). In the extracellular medium, however, conductivity is nonzero. As a consequence, the polarization potential and the current distribution will mutually influence each other.

Thus, we face the question: How do we quantitatively calculate the electric field and potential in such a medium? And what is its time dependence and frequency dependence? Looking at the temporal behavior, there are two different regimes from the biological point of view. First, there is the transitory regime which describes the short period of opening and shutting down of the source and its response of the medium with some delay. Second, there is the so-called asymptotic or permanent regime, where no current flows. These regimes will be considered in the next sections.

C. Asymptotic behavior in region 1

Let us start by considering the behavior in region 1 when the system has settled into an asymptotic regime. It means that charges move and after some time attach to the surface of the passive cell membrane (region 2). We call this a stationary or equilibrium regime. In this region, the electric properties are characterized by permittivity ϵ_1 and conductivity σ_1. We assume that these electric properties are identical everywhere inside region 1, i.e., permittivity ϵ_1 and conductivity σ_1 are constant.

To describe this situation, we start by recalling the fundamental equations of electrodynamics. Gauss' law, which relates the electric field $\vec{E}$ to the charge density ρ, reads

$$\vec{\nabla} \cdot (\epsilon_1 \vec{E}) = \rho. \tag{2}$$

Moreover, because σ_1 is constant, there is Ohm's law, which relates the electric field $\vec{E}$ to the current density $\vec{j}$,

$$\vec{j} = \sigma_1 \vec{E}. \tag{3}$$

From Maxwell's equations one obtains the continuity equation

$$\vec{\nabla} \cdot \vec{j} + \frac{\partial \rho}{\partial t} = 0. \tag{4}$$

Using Eqs. (2)–(4) and recalling that ϵ_1 and σ_1 are both constant in region 1 implies the following differential equation for the charge density:

$$\frac{\partial \rho}{\partial t} = -\frac{\sigma_1}{\epsilon_1}\rho. \tag{5}$$

A particular solution to this equation requires us to specify boundary conditions and initial conditions. Here the boundary conditions are such that the electric field (the component of the field perpendicular to the surface) on the surface of the source and on the surface of the passive cell is given (Dirichlet boundary conditions). The general solution of Eq. (5) is

$$\rho(\vec{x},t) = \rho(\vec{x},0)\exp\left[-\frac{\sigma_1}{\epsilon_1}t\right] = \rho(\vec{x},0)\exp[-t/T_{M_1}],$$

$$\rho(\vec{x},t) \underset{t\to\infty}{\to} 0, \tag{6}$$

i.e., with increasing time the charge distribution goes exponentially to zero. The time scale, which characterizes the exponential law, is Maxwell's time of relaxation, T_{M_1}. In general, it is defined by

$$T_M = \frac{\epsilon}{\sigma}. \tag{7}$$

In particular, in region 1, one has $T_{M_1} = \epsilon_1/\sigma_1$. In the limit of large time, the continuity equation implies $\vec{\nabla} \cdot \vec{j} = 0$, i.e., there

are no sources or sinks. Also in this limit the electric potential satisfies Laplace's equation, $\Delta V=0$, which follows from Gauss' law. Maxwell's relaxation time T_{M_1} in region 1 is very short, of the order of 10^{-10} s, thus the charge density tends very quickly to zero, and so does the extracellular potential.

D. Behavior in region 2

Region 2 is the near neighborhood of the membrane of a passive cell. The neuronal source creates the source field (or primary field) $\vec{E}_{source}$. As pointed out above [Fig. 1(c)], due to the presence of a source and the presence of free charges near the passive-cell membrane, there will be a polarization of the free charges, described by an electric induced field (or secondary field) $\vec{E}_{ind}$ also denoted by $\vec{E}_{free}$. Let us assume that the source field is "switched on" at time $t=0$. Such a time dependence is described by a Heaviside step function $H(t)$, given by $H(t)=1$ for $t>0$ and $H(t)=0$ for $t\leq 0$. Thus we have

$$\vec{E}_{source}(\vec{x},t)=\vec{E}_0(\vec{x})H(t). \tag{8}$$

The electric field present in region 2 results from the source field $\vec{E}_{source}$, the field due to free charges $\vec{E}_{free}$ (which create the induced field) and the field due to fixed localized charges (dipoles) of the membrane $\vec{E}_{membr}$. Under the hypothesis that the passive-cell membrane is a rigid structure with dipoles in fixed locations and under the assumption that ion channels in that membrane remain closed, we conclude that the electric field $\vec{E}_{membr}$ does not vary in time. Gauss' law and the continuity equation now read

$$\vec{\nabla}\cdot\vec{E}_{free}=\frac{\rho_{free}}{\epsilon_2},\quad \vec{\nabla}\cdot\vec{j}=-\frac{\partial\rho_{free}}{\partial t}. \tag{9}$$

Ohm's law reads

$$\vec{j}=\sigma_2(\vec{E}_{source}+\vec{E}_{free}+\vec{E}_{membr}), \tag{10}$$

which implies

$$\frac{1}{\sigma_2}\frac{\partial\rho_{free}}{\partial t}=-\vec{\nabla}\cdot(\vec{E}_{source}+\vec{E}_{free}+\vec{E}_{membr})$$

$$=-\frac{\rho_{free}}{\epsilon_2}+f(\vec{x})\quad \text{for } t>0. \tag{11}$$

While ρ_{free} depends on the position and time, the function $f(\vec{x})$ denotes a time-independent term ($\vec{E}_{membr}$ is time independent and $\vec{E}_{source}$ is time independent for $t>0$). The solution of Eq. (11) becomes

$$\rho_{free}(\vec{x},t)=a(\vec{x})+b(\vec{x})\exp[-t/T_{M_2}]\quad \text{for } t>0. \tag{12}$$

Here, $T_{M_2}=\epsilon_2/\sigma_2$ denotes the Maxwell time in region 2. The function $a(\vec{x})$ represents the free charge density at equilibrium, that is a long time ($t=\infty$) after the source has been switched on and the free charges have settled in region 1 in such a way that in region 1 no net electric field is left and hence no flow of electric current occurs. The function $b(\vec{x})$ denotes the difference of the free charge density at the moment when switching on the source and the free charge density at equilibrium. One should note that $\rho_{free}(\vec{x},t)$ is a continuous function in $\vec{x}$ at $t=0$. Poisson's equation implies that a linear relation holds between the free charge density and the induced potential. This and Eq. (12) yields

$$V_{ind}(\vec{x},t)=c(\vec{x})+d(\vec{x})\exp[-t/T_{M_2}]\quad \text{for } t>0. \tag{13}$$

In order to understand the meaning of the functions $c(\vec{x})$ and $d(\vec{x})$, let us consider as an example the following source potential:

$$V_{source}(\vec{x},t)=\beta H(t)+\alpha[1-H(t)], \tag{14}$$

where α and β are taken as constant in space and time. This source function makes a jump immediately after $t=0$. Then the induced potential becomes

$$V_{ind}(\vec{x},t)=V_{ind}^{equil}(\vec{x})+[V_{ind}(\vec{x},t=+\delta)-V_{ind}^{equil}(\vec{x})]$$
$$\times\exp[-t/T_{M_2}]\quad \text{for } t>0, \tag{15}$$

where $V_{ind}^{equil}(\vec{x})$ denotes the induced potential at equilibrium and $V_{ind}(\vec{x},t=+\delta)$ denotes the induced potential immediately after the source has been switched on. The resulting total potential is given by

$$V(\vec{x},t)=V_{source}(\vec{x},t=+\delta)+V_{ind}(\vec{x},t)\quad \text{for } t>0, \tag{16}$$

where $V_{source}(\vec{x},t=+\delta)$ denotes the source potential Eq. (14) immediately after the source has been switched on.

Now let us consider more specifically a source with time dependence given by the following function:

$$V_{source}(\vec{x},t)=\begin{cases}\beta H(t), & \text{case (a)},\\ \alpha[1-H(t)], & \text{case (b)}.\end{cases} \tag{17}$$

In case (a), the source potential is constant ($=\beta$) in space and jumps in time from 0 to 1 immediately after $t=0$, meaning the source is switched on. In case (b), the source potential is constant ($=\alpha$) in space and jumps in time from 1 to 0 immediately after $t=0$, meaning that the source is switched off. By repetition of alternate switch-ons and switch-offs, one can introduce a temporal pattern with a certain frequency, as shown in Fig. 2(a). Here we are interested in the temporal behavior of the induced potential under such circumstances. In case (a) Eq. (15) implies for the induced potential the following relation:

$$V_{ind}(\vec{x},t)=V_{ind}^{equil}(\vec{x})(1-\exp[-t/T_{M_2}])\quad \text{for } t>0. \tag{18}$$

By a differentiation, one finds that the induced potential obeys the following differential equation:

$$\frac{\partial V_{ind}(\vec{x},t)}{\partial t}+\frac{1}{T_{M_2}}V_{ind}(\vec{x},t)=\frac{1}{T_{M_2}}V_{ind}^{equil}(\vec{x}). \tag{19}$$

Similarly, in case (b) one obtains for the induced potential

$$V_{ind}(\vec{x},t)=V_{ind}(\vec{x},t=o)\exp[-t/T_{M_2}]\quad \text{for } t>0, \tag{20}$$

which obeys the following differential equation:

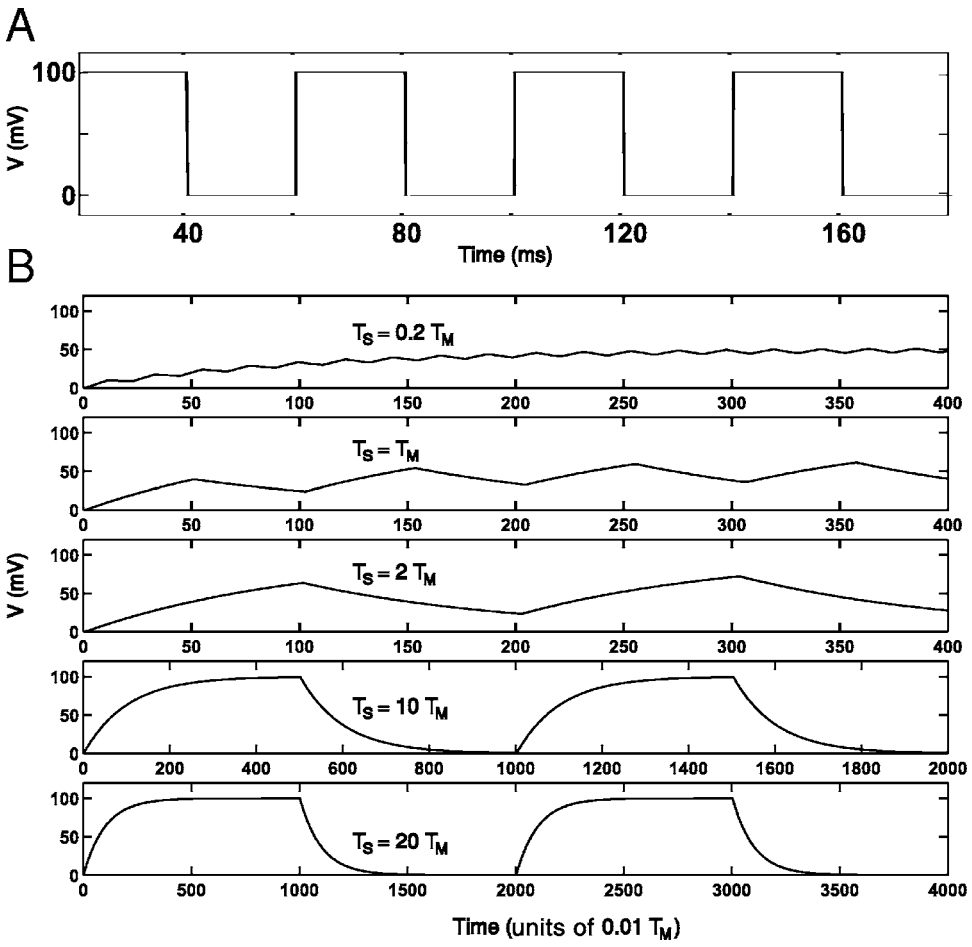

FIG. 2. Time dependence of an induced electric potential in response to an external source given by a periodic function. (a) Source potential given by a periodic step function $H(\sin(\omega t))$, with period $T_S = 2\pi/\omega = 80$ ms. (b) Induced electric potential for various values of T_S/T_M. In the case $T_S/T_M \ll 1$ (top), the induced potential fluctuates closely around the mean value of the source potential. In the case $T_S/T_M \gg 1$ (bottom) the induced potential relaxes and fluctuates between $V_{min} = 0$ mV and $V_{max} = 100$ mV of the source potential. As a result, the amplitude of the oscillation becomes more attenuated with increased frequency $f = 1/T_S$.

$$\frac{\partial V_{ind}(\vec{x},t)}{\partial t} + \frac{1}{T_{M_2}} V_{ind}(\vec{x},t) = 0. \tag{21}$$

Equations (19) and (21) can be expressed as

$$\frac{\partial V_{ind}(\vec{x},t)}{\partial t} + \frac{1}{T_{M_2}} V_{ind}(\vec{x},t) = \frac{1}{T_{M_2}} f(\vec{x}) H(t),$$

$$f(\vec{x}) = \begin{cases} V_{ind}^{equil}(\vec{x}), & \text{case (a)}, \\ 0, & \text{case (b)}. \end{cases} \tag{22}$$

In order to solve this differential equation, one has to know the function $f(\vec{x})$ given by $V_{ind}^{equil}(\vec{x})$ in case (a). How to obtain this function? We consider the case of an ideal dielectric medium in region 1. The function $V_{ind}^{equil}(\vec{x})$ is related to the full potential and the source potential via

$$V_{ind}^{equil}(\vec{x}) = V_{tot}^{equil} - V_{source}^{equil}(\vec{x}). \tag{23}$$

The resulting total potential at equilibrium V_{tot}^{equil} on the surface of the membrane will be constant in time and in space (on the membrane surface), i.e., independent of position $\vec{x}$, because otherwise there would be a flow of charges. The value of V_{tot}^{equil} can be found by computing

$$\int_S d\vec{S} \cdot \epsilon_1 \vec{E}_{tot}^{equil} = Q_{tot}^{equil}. \tag{24}$$

The integral is done over any surface S in the extracellular fluid, chosen such that it only includes the passive cell. Q_{tot}^{equil} is the total charge in the interior of such a surface S. The physical value of V_{tot}^{equil} must be such that the corresponding electric field $\vec{E}_{tot}^{equil}$ yields $Q_{tot}^{equil} = 0$ via Eq. (24), because the total charge of the passive cell before switching on the source was neutral.

Note that the above reasoning is valid for an ideal dielectric medium, which is not the case for extracellular media. However, the small amplitude of the currents involved ($\sim$100 pA), the value of conductivity of extracellular fluid ($\sim$3.3 S/m), the small dimension of most passive cells ($\sim$10 μm diameter; $\sim$2 nm of membrane thickness), and the high resistivity of membranes, imply a weak voltage drop on cell surfaces due to the current. Thus, the electrostatic induction is very close to an ideal dielectric.

E. Source given by periodic step function: An equivalent *RC* electric circuit

We considered above initial conditions where the source potential has been switched on at some time. This can be directly generalized such that the temporal behavior of the source potential is given by a periodic step function, with a

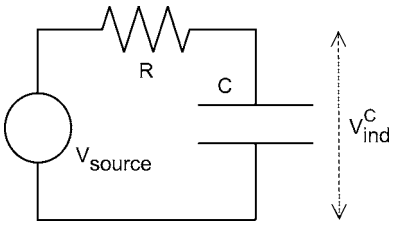

FIG. 3. Model of an electric circuit with capacitor C, resistor R. V_{source} denotes the potential of the source and V^C_{ind} denotes the induced potential at the capacity C.

period T_S, as shown in Fig. 2(a). The corresponding induced potential, presented in Fig. 2(b), shows a piecewise exponential increase followed by an exponential decrease. The figure shows the response to a source of a periodic step function, for different values of T_S measured in units of T_M. One observes the following behavior. At the top of the figure the period T_S is smallest, i.e., which corresponds to a rapid oscillation about its time average. At the bottom of the figure the period T_S is largest, corresponding to a low-frequency oscillation. It is important to note that the amplitude of oscillation (i.e., the difference between its maximal and minimal value) is much smaller for small T_S than for large T_S. This yields an attenuation effect of high frequencies in the induced potential.

Such behavior of the induced potential is well known from and mathematically equivalent to that of an RC electric circuit, with a resistor R and a capacitor C (see Fig. 3). The equation of motion in such an RC circuit relating the induced potential V^C_{ind} to the capacity C to the source potential V_{source} is given by

$$\frac{\partial V^C_{ind}(t)}{\partial t} + \frac{1}{RC} V^C_{ind}(t) = \frac{1}{RC} V_{source}(t). \tag{25}$$

This equation is mathematically equivalent to Eq. (22), if we identify

$$V_{ind}(\vec{x},t) \leftrightarrow V^C_{ind}(t), \quad V^{equil}_{ind}(\vec{x})H(t) \leftrightarrow V_{source}(t),$$

$$\frac{1}{\sigma} \leftrightarrow R, \quad \epsilon \leftrightarrow C, \quad T_M \leftrightarrow RC. \tag{26}$$

Thus, for each point $\vec{x}$ near the membrane of a passive cell [region 2 in Fig. 1(a)], we can set up an equivalent electric circuit, which is equivalent in the sense that it gives a differential equation with the same mathematical solution as for the induced potential of the original system of a source and a passive cell.

F. Induced potential for time-dependent source and transfer function from Fourier analysis

The analog of an RC electric circuit can be used to determine the characteristic properties of the source and/or passive-cell system, like the cutoff frequency. For that purpose let us consider the source potential to be given by a periodic function of a sinusoidal type switched on at time $t=0$:

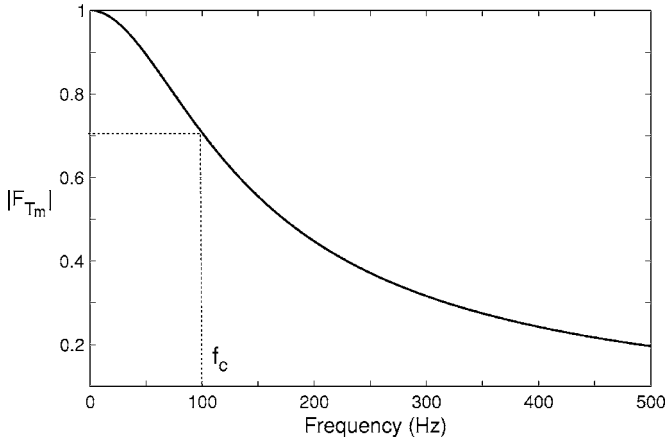

FIG. 4. Modulus of a transfer function vs frequency, using biologically realistic parameters ϵ and σ.

$$V_{source}(\vec{x},t) = V_0(\vec{x})\exp(i\omega t)H(t). \tag{27}$$

The corresponding induced potential in our model obeys Eq. (22), which can be written in the form

$$\frac{\partial V^{ind}(\vec{x},t)}{\partial t} + \frac{\sigma}{\epsilon} V^{ind}(\vec{x},t) = \frac{\sigma}{\epsilon} V^0(\vec{x})H(t)\exp(i\omega t). \tag{28}$$

It can be shown that the large-time asymptotic behavior of the solution $V^{ind}(\vec{x},t)$ is given by

$$V_{ind}(\vec{x},t) \underset{t\to\infty}{\sim} \frac{\sigma}{\sigma + i\omega\epsilon} V_0(\vec{x})\exp(i\omega t). \tag{29}$$

The asymptotic behavior enters also into the transfer function. The transfer function is obtained from the Fourier transformation of the temporal behavior of the induced potential. It is defined by the ratio of induced potentials corresponding to frequency ω of the source over the induced potential at frequency $\omega=0$ of the source, by the following expression:

$$F_{TM}(\vec{x},\omega) = \lim_{t\to\infty} \frac{V^{\omega}_{ind}(\vec{x},t)\exp(-i\omega t)}{V^{\omega=0}_{ind}(\vec{x},t)}. \tag{30}$$

Comparing Eqs. (29) and (30), we obtain

$$F_{TM}(\omega) = \frac{1}{1 + i\omega\epsilon/\sigma}. \tag{31}$$

F_{TM} is a complex function, with modulus

$$|F_{TM}(\omega)| = \frac{1}{\sqrt{1 + (\omega\epsilon/\sigma)^2}}. \tag{32}$$

For frequency zero one has $|F_{TM}|=1$. The cutoff frequency f_c is defined such that $|F_{TM}|$ falls off to the value $|F_{TM}| = 1/\sqrt{2}$. Thus we find

$$f_c = \frac{\omega_c}{2\pi} = \frac{\sigma}{2\pi\epsilon} = (2\pi T_M)^{-1}. \tag{33}$$

The modulus of the transfer function vs frequency is shown in Fig. 4, for the case of parameters σ and ϵ of region 2, as given in Sec. II A. This corresponds to a cutoff frequency $f_c=100$ Hz. Such a behavior represents a frequency filter. It

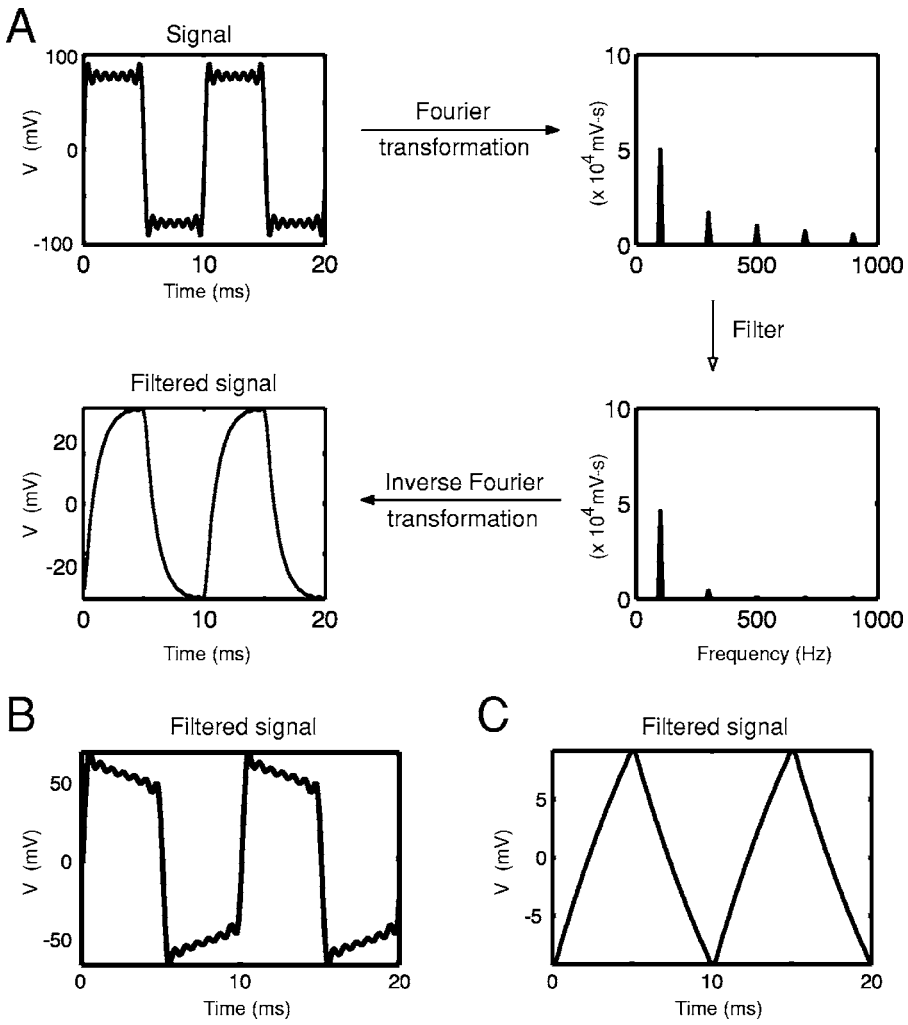

FIG. 5. Effect of the filtering of a periodic electrical potential representing a neural source. (a) The original signal (top row, left panel). The frequency spectrum of such a signal is obtained by Fourier transformation (top row, right panel). Then the signal is sent through a filter (middle row, right panel). After an inverse Fourier transformation the filtered signal as a function of time is obtained (middle row, left panel). The period of the original signal is 10 ms, and the relaxation time of the filter is 10 ms. (b) Same signal as in (a) filtered using a relaxation time of 1 ms. (c) Same signal as in (a), filtered using a relaxation time of 100 ms.

shows that we can compute the induced potential as a function of frequency based on the analogy with an equivalent electric circuit with a resistor R and capacity C arranged in serial order. A series of detailed numerical simulations, modeling frequency filtering of extra-cellular neural tissue in the neighborhood of passive cells in terms of the electric circuit model, Eq. (25), using physiologically realistic parameters of ϵ and σ are shown in Fig. 5. They present the signal coming from a periodic step function with a period $T_S=10$ ms, i.e., a frequency of 100 Hz. Going from Fig. 5(a) to Fig. 5(c) T_S is kept fixed but T_M increases, i.e., T_S/T_M decreases. Figure 5(a) corresponds to the case where the relaxation time T_M is 10 times smaller than the period of the signal T_S. In Fig. 5(b) T_M and T_S are equal, and in Fig. 5(c) T_M is 10 times larger than T_S. We observe that the shape of the signal after filtering is more or less intact for $T_S/T_M=10$ and becomes gradually more deformed when going over to $T_S/T_M=0.1$. As the Fourier transformation after filtering shows, the higher frequency components get gradually more suppressed. This represents a low-frequency band pass.

To close this section, we would like to remark that the treatment above is general and not restricted to step functions. The Heaviside functions were used as a tool to distinguish transient and asymptotic behaviors, as well as to calculate the transfer function. For an arbitrarily complex time-dependent source, the convolution integral with this transfer function gives the filtered signal, so this approach can be applied to any physical signal.

III. MODELING FREQUENCY DEPENDENCE OF MULTIPLE NEURONS AND PASSIVE CELLS

In Sec. II, we laid out the theoretical framework of the model and showed that this model—with respect to time and frequency dependence but neglecting spatial dependence—is equivalent to a *RC*-circuit model. As an example, we have presented numerical simulations treating the case of a single source and a single passive cell. In this section, we would like to generalize this approach to take into account space and time dependence in LFPs. In this and the following section, we present numerical simulations considering more complex three-dimensional arrangements of neuronal sources and passive cells.

A. Computation of field potentials for multiple neurons and passive cells

In a first set of numerical simulations, we considered three-dimensional arrangements of sources and passive cells. To solve the equations, we used a discretization method simi-

lar to the finite element methods (see below). The neuron source was represented by a cubic shape of length L_{neuron}, and likewise, we consider the passive cells being represented by cubes of length L_{pass}. Neuron source and passive cells were located at some distance d from each other. Although being far from realistic, this geometry facilitates numerical simulations. Since the aim of this work is not to make quantitative predictions, such an arrangement will help explaining qualitatively the frequency attenuation properties of field potentials in three-dimensional (3D) arrangements of cells, as we will show below.

Let us first outline the method of the numerical computation of the potential. From a mathematical point of view, the solution of a partial differential equation is required to specify suitable boundary conditions. In the context of Maxwell's equations, Dirichlet's boundary conditions (potential given on a closed surface) or von Neumann's boundary conditions (electric field given on a closed surface) are known to guarantee a unique solution. Here, we suggest using the boundary condition of Dirichlet's type, that is we assume that the potential is given on the surface of all cells. The problem is, however, that the value of the physical potential on the surface of those cells is not known *a priori*, and, moreover, the functional values of the potential cannot be chosen freely. The physical solution is determined by the principle that all free charges are located such that the electromagnetic field energy becomes minimal (Thomson's theorem). This imposes constraints on the boundary conditions.

How can we figure out those *a priori* unknown boundary conditions? We use the physical principle that those physical boundary conditions are equivalent to the condition that Gauss' integral summing the flux around a charge source becomes invariant when the integration surface is changed. A computational strategy to find those boundary conditions is to use a variational principle, starting from some initial guess of boundary conditions and then to adjust iteratively the boundary conditions until eventually the total electric energy attains its minimum.

We used a variational principle via the following iterative scheme. In the first step, we compute the potential due to the source in the absence of any passive cell in the asymptotic regime (a long time after the source has been switched on), for the case where the source has no frequency dependence ($\omega=0$). We assume that the potential obeys the boundary condition on the surface of the neuron source

$$V(\vec{x}) = V^0 = \text{const} \quad \text{for } \vec{x} \text{ on the surface of the source.} \tag{34}$$

The potential satisfies Laplace's equation

$$\Delta V(\vec{x}) = 0. \tag{35}$$

The numerical solution has been carried out using the standard method of relaxation.

In the second step, we place a passive cell at some distance d from the neuron source. We want to calculate the induced potential due to the presence of the passive cell. We proceed in the following way. Let us consider for a moment that the passive cell is small compared to the size of the neuron, $L_{pass} \ll L_{neuron}$. Then the induced potential on the surface of the passive cell would be almost identical to V_{pass}^{center}, the potential created by the source alone, evaluated at the center of the passive cell. Then imposing the boundary condition that the potential on the surface of the passive cell takes the value V_{pass}^{center} would be very close to the exact solution. Now we no longer consider the passive cell as tiny. Then imposing the boundary condition boundary on the surface of the passive cell

$$V(\vec{x}) = V_{pass}^{center} = \text{const} \quad \vec{x} \text{ on a surface of a passive cell} \tag{36}$$

becomes an approximation.

In the third step, taking into account that the potential obeys the boundary conditions on the neuron source and on the passive cell, Eqs. (34) and (36), we solve again Laplace's equation, Eq. (35). Now we will test if the obtained solution $V(\vec{x},t)$ is the correct solution. Using Gauss' theorem, one has

$$\int_{S_{neuron}} d\vec{s} \cdot \vec{E} = \int_{S_{neuron+pass}} d\vec{s} \cdot \vec{E}. \tag{37}$$

Here the integral denotes an integral over a closed surface, first englobing the neuron source and second englobing the neuron source plus the passive cell. Because the passive cell has a total charge $Q_{pass}=0$, Eq. (37) should be satisfied by the physical solution $V_{phys}(\vec{x},t)$. As long as $V(\vec{x},t)$ differs from $V_{phys}(\vec{x},t)$, one has to adjust the potential on the surface of the passive cell, solve again Laplace's equation, and verify the charge balance Eq. (37). This is an iterative process, which turned out to converge quite fast towards the physical solution.

This method can be applied as well to treat multiple neuron sources and multiple passive cells. We would like to point out that the extracellular neural tissue is composed of much more passive cells than neurons. On average the number of glial cells per unit volume is higher than the number of neurons per unit volume by about a factor of 10. The physical consequence of this property is that the induced potential due to the presence of passive cells becomes more important than the source potential.

Finally, to investigate the effect of time-dependent sources and multiple passive cells, we take advantage of the following equivalence: the induced potential on a cell with a relaxation time T_M subject to a time-dependent source is equivalent to the induced potential in a cell with $T_M=0$ subject to a "filtered" source given by the convolution of the source with the transfer function [F_{TM} in Eq. (30)]. This corresponds to the following calculation steps, for each passive cell: (1) evaluate the source $S(\vec{x},\omega)$ provided by the neighboring system of sources and other passive cells; (2) evaluate the filtered source $S^*(\vec{x},\omega)=S(\vec{x},\omega)F_{TM}(\omega)$ [from Eq. (31)]; (3) calculate the induced potential on the passive cell using a similar procedure as outlined above for a time-independent source ($\omega=0$). The whole procedure is repeated iteratively until all sources and induced potentials converge towards the physical solution. Numerical results using this iterative procedure are presented in the next section.

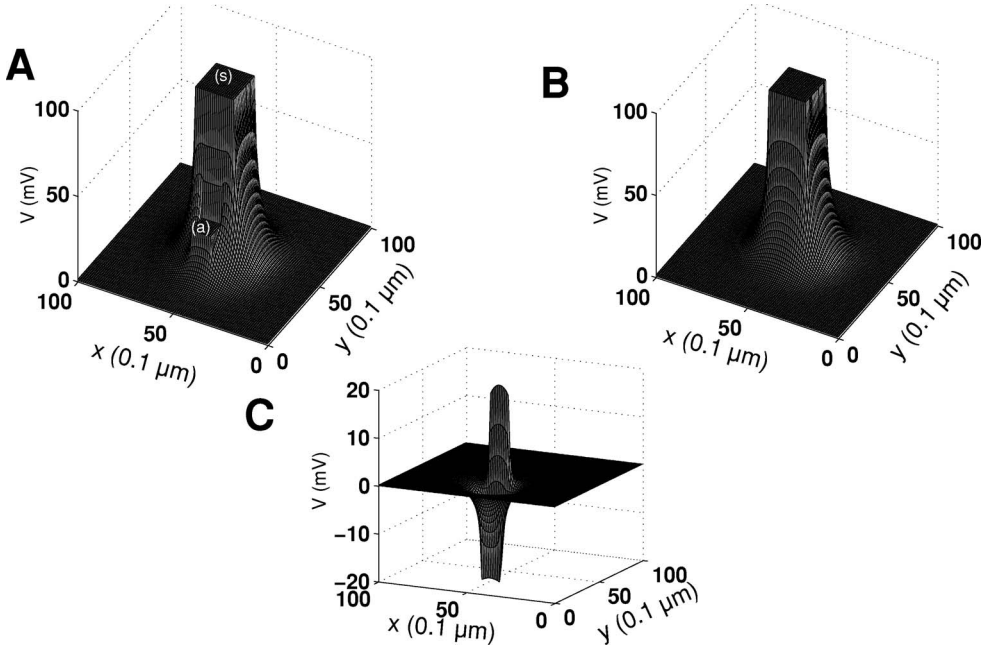

FIG. 6. Extracellular potential generated by a time-independent source situated nearby a passive cell. Both the source (s) and the passive cell (a) have a cubic shape; the passive cell was twice smaller than the source. (a) Total extracellular electric potential ($V_{source}+V_{ind}$) in a horizontal plane cut at the base of both cells. (b) Electric potential resulting from the source only (V_{source}). (c) Induced electric potential (V_{ind}). All potentials were obtained by solving Laplace's equation with a static source ($f=0$), and are represented in units of a percent of the source potential. The distance is represented in units of 0.1 μm.

It is important to note that in the range of frequencies considered here, the wavelengths are too large for significant wave propagation phenomena. Accordingly, we only consider sources where space and time dependences factorize. Consequently, the transfer function does not have any space dependence. In addition, the application of the transfer function holds for spherical sources as well as for cubic sources.

B. Numerical results

We now present results of numerical solutions of Laplace's equation for the scenario in the presence of a source and several passive cells. We have taken as parameters of conductivity and permittivity those corresponding to the intracellular space at the membrane of the passive cell, given in Sec. II A (conductivity is nonzero). It corresponds to a cutoff frequency of $f_c=100$ Hz. The corresponding Maxwell time and transfer function are obtained by Eqs. (33) and (31).

The goal is to show that the induced potential gives an important contribution to the total, i.e., physical potential. The results are presented in Figs. 6–9. For the case of a single source and a single passive cell the source potential,

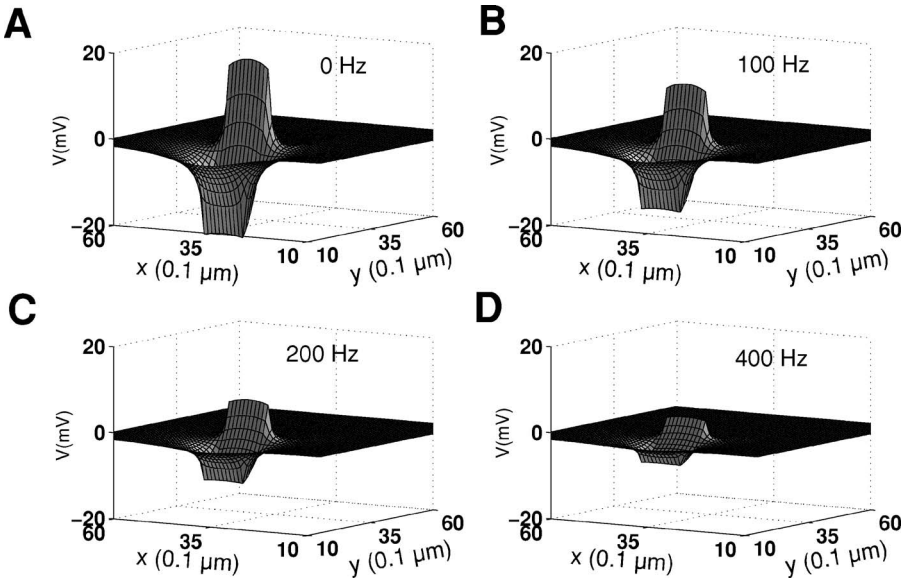

FIG. 7. Same as Fig. 6, but showing the induced potential V_{ind} for a time-dependent source [frequencies $f=0,100,200,400$ Hz in (a), (b), (c), (d), respectively]. The induced potential tends to zero when f increases.

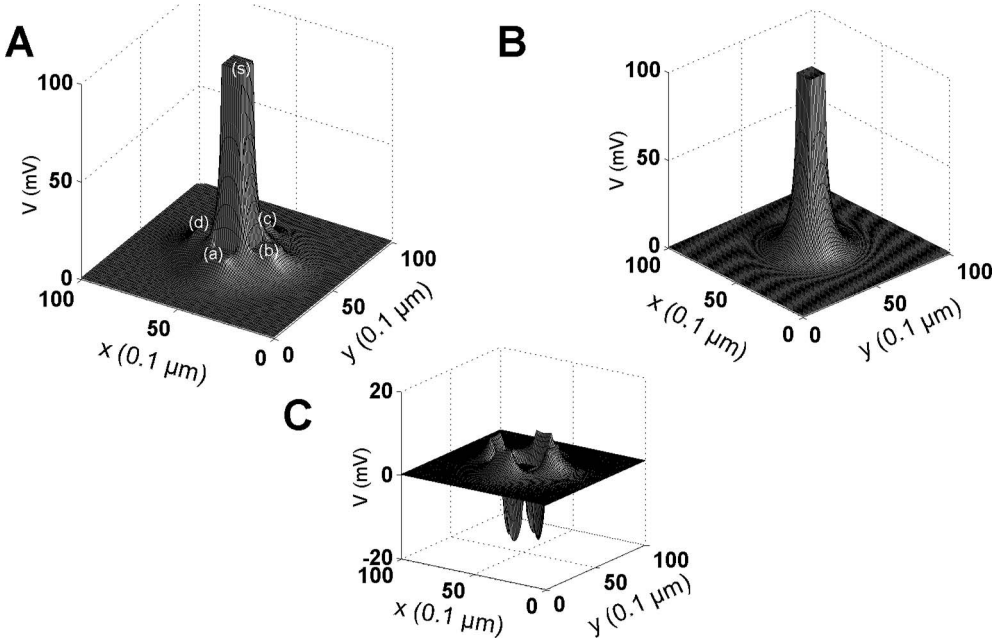

FIG. 8. Extracellular potential generated by a time-independent source surrounded by six passive cells. Same description as in Fig. 6, but for a system of a single static source (s) and six passive cells. The figure shows the potential in a horizontal plane in which four passive cells are visible (a). (a) Total extracellular potential; (b) source electric potential; (c) induced electric potential V_{ind}.

the induced potential, and the total potential are shown in Figs. 6(a)–6(c), respectively. Comparing the source potential (b) with the induced potential (c), one observes that the latter gives a substantial contribution. In Figs. 7(a)–7(d) we show the induced potential multiplied with the norm of the transfer function. We observe that the frequency-dependent induced potential decreases when the frequency of the source increases from 0 to 400 Hz. Figures 8 and 9 show the corresponding results in the case of a single source and four passive cells. We observe qualitatively the same results as in Fig. 6. These results demonstrate clearly the phenomenon of attenuation of high frequencies in the induced potential. It should be mentioned that the computations were carried out in 3D, but are depicted as a projection in 2D. Qualitatively the same results are obtained in the case of two sources and a single passive cell (not shown). Again we found that for the time-independent source the induced potential is nonnegligible compared to the source potential and the frequency-dependent induced potential rapidly decreases when the frequency goes from 0 to 400 Hz.

IV. ATTENUATION AS A FUNCTION OF DISTANCE

The simulations shown in the preceding section illustrated the fact that the induced potential vanishes for very high frequencies of the source field, a fact that can also be deduced from Eq. (22). In other words, for very high frequencies ($\gg T_M^{-1}$), the extracellular field will be equal to the

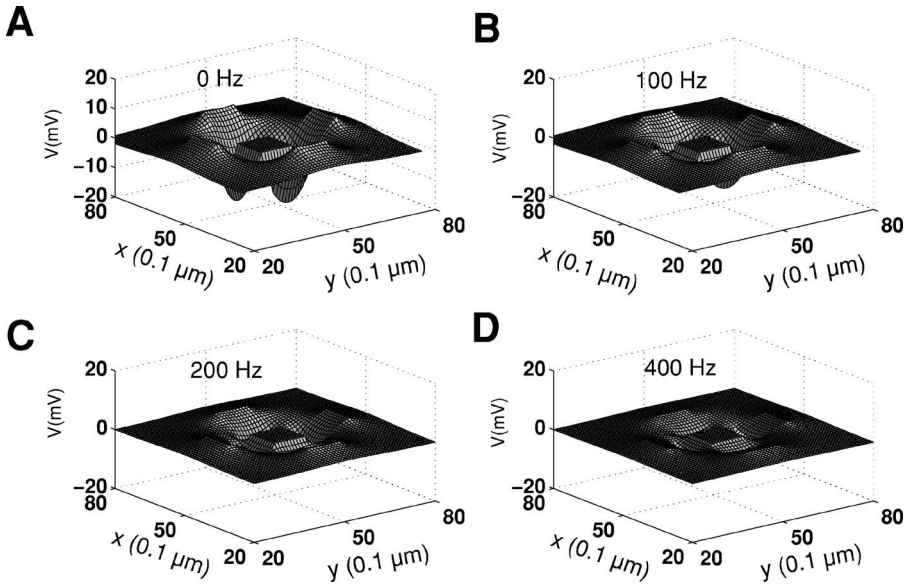

FIG. 9. Same as Fig. 8, but showing the induced potential V_{ind} for a time-dependent source at different oscillation frequencies [f=0,100,200,400 Hz in (a), (b), (c), (d), respectively].

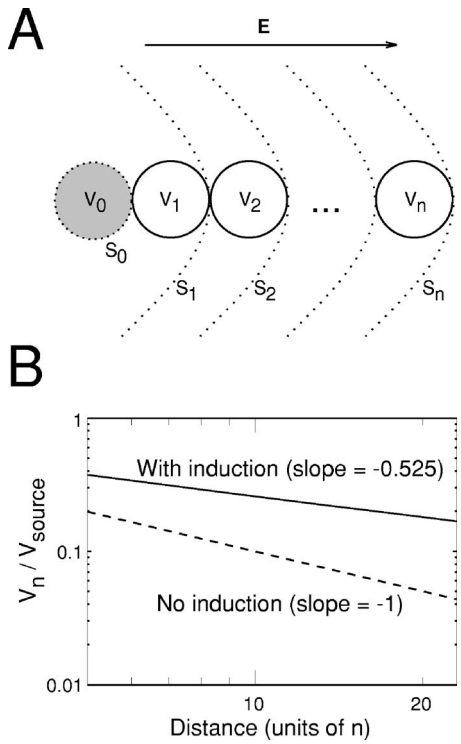

FIG. 10. Extracellular potentials as a function of distance for a system of densely packed spherical cells. (a) Scheme of the arrangement of successive layers of identical passive cells packed around a source (in gray). The potential of the source is indicated by V_0. $V_1, V_2, \ldots, V_n$ indicate the potential at the surface of passive cells in layers $1, 2, \ldots n$, respectively. The dotted lines indicate isopotential surfaces, which are concentric spheres centered around the source, and which are indicated here by $S_1, S_2, \ldots, S_n$. (b) Extracellular potential as a function of distance (in units of a cell radius), comparing two cases: with induction (solid line, corresponding to the arrangement schematized in (a)], and without induction (dashed line, source surrounded by conductive fluid only). Both cases predict a different scaling of the electric potential with a distance (see text for details).

source field, since the induced field will vanish. The space dependence is easy to deduce in such a case, and the extracellular potential attenuates with distance according to a $1/r$ law, as if the source was surrounded only by conducting fluid.

However, for very low frequencies ($\ll T_M^{-1}$), the space dependence of the extracellular potential will be a complex function depending on both the $1/r$ attenuation of the source field, and the contribution from the induced field. Such a space dependence is not easy to deduce, since it depends on the spatial arrangement of fluids and membranes around the source. In this section, we attempt to derive such a low-frequency space dependence for a more realistic system of densely packed cells [illustrated in Fig. 10(a)]. To constrain the behavior to low frequencies, we only consider the zero-frequency limit by using a constant source field. We proceeded in two steps. First, we calculated the electric potential at the surface of a passive cell (Sec. IV A). Second, we calculated the spatial profile of LFPs in a system of densely packed spheres of identical shape (Sec. IV B).

A. Electric potential at the surface of passive membranes at equilibrium

Let us assume that a spherical passive cell is embedded in a perfect dielectric medium, and is exposed to a constant electric field. At equilibrium, we have seen above that the effect of the electric field is to polarize the charge distribution at the surface of the cell, such as to create a secondary electric field [see Fig. 1(b)], but the induced electric field is zero inside the cell. In this case, the conservation of charges on the surface implies

$$\int \int_{Surf} \rho_{Surf} dS = 0, \tag{38}$$

where ρ_{Surf} is the charge density on the surface of the cell. The resulting electric potential is given by

$$V_{tot}(x,y,z) = V_{source}(x,y,z) + \int \int_{Surf} \frac{\rho_{Surf}}{4\pi\epsilon r} dS, \tag{39}$$

where V_{source} is the electric potential due to the source field, V_{tot} is the total resulting electric potential due to the source field and the induced field, and r is the distance from point (x,y,z) to the center of the cell. Because at the center of the cell, (a,b,c), we necessarily have $r=R$ (where R is the cell's radius), the value of the resulting electric potential at the center is given by

$$V_{tot}(a,b,c) = V_{source}(a,b,c) + \int \int_{Surf} \frac{\rho_{Surf}}{4\pi\epsilon R} dS$$

$$= V_{source}(a,b,c). \tag{40}$$

Thus, the electric potential at the surface of a spheric passive cell at an equilibrium equals the potential due to the primary field at the center of the cell. In other words, the effect of the secondary field in this case perfectly compensates the distance dependence of the primary field, such as the surface of the cell becomes isopotential, as discussed above.

B. Attenuation of an electric potential in a system of packed spheres

Keeping the assumption of a constant electric field, we now calculate how the extracellular potential varies as a function of distance in a simplified geometry. We consider a system of packed spheres as indicated in Fig. 10(a). From the solution of Laplace's equation, the extracellular potential at a distance r from the source center is given by

$$V(r) = \frac{k}{r}, \tag{41}$$

where k is a constant, which is evaluated from the potential at the surface of the source [S_0 in Fig. 10(a)]:

$$V(R) = V_0 = \frac{k}{R}, \tag{42}$$

where R is the radius of the source. Thus, the potential due to the source field at a given point r in extracellular space is given by

$$V(r) = \frac{RV_0}{r}. \tag{43}$$

Considering the arrangement of Fig. 10(a), if all cells of a given layer are equidistant from the source, their surface will be at the same potential (see Sec. IV A), which we approximate as a series of isopotential concentric surfaces [S_1, $S_2, \ldots, S_n$ in Fig. 10(a)]. A given layer (n) of isopotential cells is therefore approximated by a new spherical source of radius r_n, which will polarize cells in the following layer ($n+1$). According to such a scheme, the potential in layer $n+1$ is given by

$$V_{n+1} = \frac{r_n V_n}{d_{n+1}}, \tag{44}$$

where d_{n+1} is the distance from the center of cells in layer ($n+1$) to the center of the source. According to the scheme of Fig. 10(a), we have $r_n=(2n+1)R$ and $d_n=2nR$. Thus, we can write the following recurrence relation:

$$V_{n+1} = \frac{2n+1}{2n+2} V_n. \tag{45}$$

Consequently

$$V_{n+1} = \left(\prod_{j=1}^{n} \frac{2j+1}{2j+2} \right) V_0, \tag{46}$$

which can be written, for large n

$$V_n = \frac{(2n+1)!}{2^{2n}(n+1)!\,n!} V_0 \approx \frac{2(2n)!}{2^{2n}(n!)^2} V_0. \tag{47}$$

Using Stirling's approximation, $n! \simeq (n/e)^n \sqrt{2\pi n}$ for large n, leads to

$$V_n \simeq \frac{2}{\sqrt{\pi n}} V_0. \tag{48}$$

Thus, in a system of densely packed spherical cells, the extracellular potential falls off like $1/\sqrt{r}$ [Fig. 10(b), continuous line].

In contrast, in the absence of passive cells in extracellular space, the electric potential is given by the source field only [Eq. (43)], which, using the same distance notations as above, is given by

$$V_{n+1} = \frac{V_0}{2(n+1)}. \tag{49}$$

Such $1/r$ behavior is illustrated in Fig. 10(b) (dashed line). Note that other theories predict a steeper decay. For instance, the Debye-Hückel theory of ionic solutions [24] predicts a fall-off as $\exp(-kr)/r$.

Thus, for this particular configuration, there is an important difference in the attenuation of an extracellular potential with distance. The extracellular potential in a system of densely packed spheres falls off approximately like $1/\sqrt{r}$, in contrast to a $1/r$ behavior in a homogeneous extracellular fluid. Note that a $1/\sqrt{r}$ behavior can also be found in a system in which the source is defined as a current. For a constant current source I_0, with variations of conductivity following a spherical symmetry around the source, the extracellular potential is given by [18]

$$V(r) = \frac{I_0}{4\pi} \int_r^\infty \frac{1}{r^2 \sigma(r)} dr, \tag{50}$$

where $\sigma(r)$ is the radial profile of conductivity around the source. Assuming that $\sigma(r)=\sigma_0/\sqrt{r}$, gives

$$V(r) = \frac{\sigma_0 I_0}{4\pi\sqrt{r}} = \sqrt{\frac{R}{r}} V_0. \tag{51}$$

Consequently, the $1/\sqrt{r}$ behavior found above is functionally equivalent to a medium with conductivity varying like $1/\sqrt{r}$. This "effective conductivity" is similar to that introduced in a previous study [18].

V. DISCUSSION

From theoretical considerations and numerical simulations we have obtained the following main results: (i) We explored the assumption that neuronal current sources polarize neighboring cells. This polarization produces an induced electric field, which adds to the electric field directly produced by the sources. This induced field is non-negligible for biologically realistic parameters. (ii) This induced electric field has strong frequency-dependent properties. This system is equivalent to an equivalent *RC* circuit and always has low-pass filtering properties. (iii) The cutoff frequency of this low-pass filter is determined by Maxwell's relaxation time of the membrane surfaces surrounding neuronal sources. (iv) Consequently, the attenuation of high frequencies will not be influenced by this induced field, and will be the same as if neurons were embedded in a homogeneous extracellular medium. On the other hand, the attenuation of low frequencies will depend on the induced field, and will, therefore, depend on the geometry of fluids and membranes in the extracellular space.

In our previous work, we showed that inhomogeneities of conductivity or permittivity in extracellular space could give rise to strong frequency filtering properties [18]. However, low-pass or high-pass filters could be obtained depending on the profiles of conductivity used in this model. In the present model, a low-pass filter is predicted, consistent with experiments (which never evidenced a high-pass filter). However, the fact that frequency filtering properties are due to the alternance of high-conductive fluids and low-conductive membranes in the present model is compatible with the inhomogeneity of conductivity postulated in the previous model. One main difference with the previous model is that here, we explicitly considered a nonzero charge density on neighboring membranes.

Another similarity with the previous model concerns the mechanism of the attenuation of LFPs with distance. The primary or source field experiences a steep attenuation for all frequencies, and the electric potential will attenuate with a distance r following a $1/r$ law, similar to the attenuation in a homogeneous conducting fluid [1]. On the other hand, the

induced field will be subject to a different law of attenuation with distance, which will depend on the spatial arrangement of passive cells around the source. In the previous model it depended on the particular conductivity profile [18]. In general, for densely packed cellular membranes around the source, one will have a law of attenuation which will be of $1/r^{\alpha}$, where $\alpha<1$ may depend on the frequency ω. For example, we found $\alpha\sim 0.5$ for spherical cells in Fig. 10 for low ω. Thus, both models predict the following scenario: high frequencies follow an attenuation in $1/r$, similar to a homogeneous extracellular fluid, but low frequencies follow a slower attenuation profile, because these frequencies are "transported" by the induced field.

It should be noted that this model represents a strong approximation of the actual complexity of the mechanisms involved in the LFP generation. A first approximation was to consider passive cells as spheres, neglecting their morphological complexity. Another assumption was that the electric field results only from neuronal current sources, while other cell types, such as glial cells, also contain ion channels and may influence LFPs. A third approximation was to neglect the effect of variations of extracellular ionic concentrations (like potassium buffering by glial cells), which may also influence LFP activity, especially at low frequencies (in addition to local variations of conductivity). It is difficult to estimate the consequences of these different approximations, but the polarization effects described here should occur in more complex situations, so it is likely that the present considerations apply to more complex geometries and current sources. This should be tested by numerical simulations, for example, by constraining the model with 3D reconstructions of extracellular space from electron microscopic measurements.

The scenario outlined above of a transport of low frequencies can be tested experimentally in different ways. First, measuring the decay of specific frequency components of LFPs with distance, and, in particular, how they differ from the $1/r$ law, should yield direct information on how much extracellular space deviates from a homogeneous conducting fluid. The attenuation profile should also depend on the spatial arrangement of successive fluids and membranes in the extracellular fluid. It is conceivable to inject sinusoidal currents (of low amplitude to allow induction effects) of different frequencies using a microelectrode and measure the LFP produced at increasing distances, to obtain the law of attenuation as a function of frequency [i.e., $\alpha(\omega)$]. The comparison with model predictions should tell us to what extent the model predicts the correct attenuation.

The equivalent *RC* circuit investigated above also deserves some comment. It is well known that an electric circuit consisting of a resistor and a capacitor, which stores electric energy, introduces a phase difference between current and potential, and has characteristic low-pass filtering properties. The fact that such a simple *RC* circuit may be used as a model of frequency filtering of cerebral tissue is, however, more surprising. In fact, if we construct an arrangement of densely packed passive cells around a current source [such as in Fig. 10(a)], the system will be equivalent to a series of RC circuits, each representing one "layer" of cells. In this context, it may be interesting to relate the type of spatial arrangement to type of equivalent circuit(s) obtained, for example by considering different cases such as cells or random diameters, various shapes, or even by using 3D morphological data from real brains obtained by serial reconstructions from electron microscopy. This type of investigation constitutes a possible extension of the present work. In addition, we have considered a source being given by a single neuron. In reality, the source of LFP activity is a system of many neurons with complicated phase relationships between their activities. An extension of our model in this direction would also be a most important step to take.

A second model prediction that should be testable experimentally concerns the predicted cutoff frequency. This information can be related to experimentally recorded LFPs which could be analyzed using the Fourier analysis to yield information about the cutoff frequency. However, such an analysis should be done by comparing different network states, to make sure that the cutoff frequency is not dependent on activity but rather depends on structural parameters. If correctly done, this analysis should provide an estimate of the Maxwell's relaxation time for the surface of membranes, or equivalently the tangential conductivity of membrane, for which there exists presently no experimental measurement. Work in this direction is under way.

Finally, we would like to conclude by suggesting that these theoretical predictions in conjunction with measurements of frequency-dependent field potentials may lead to new ways for detecting anomalies, for example, due to degenerative diseases such as Alzheimers or brain tumors. If such diseases cause structural changes in brain tissue, e.g., the creation of vacuoles, this will manifest itself by changes of electric properties like the attenuation of low-frequency components with distance. These changes should be visible in measurements of EEG, ECoG, or LFP signals from multielectrodes in the area of affected brain tissue. Detecting such changes supposes a prior understanding of the spectral filtering properties of these electric signals, which is one of the main motivations of the present work.

ACKNOWLEDGMENTS

H.K. is grateful for support by NSERC Canada. A.D. has been supported by CNRS and HFSP. We acknowledge discussions with Yves DeKoninck and Arnaud Delorme.

[1] P. L. Nunez, *Electric Fields in the Brain. The Neurophysics of EEG* (Oxford University Press, Oxford, UK, 1981).
[2] *Electroencephalography*, 4th ed., edited by E. Niedermeyer and F. Lopes da Silva (Williams and Wilkins, Baltimore, MD, 1998).
[3] B. Hille, *Ionic Channels of Excitable Membranes* (Sinauer Associates, Sunderland, MA, 1992).
[4] D. Johnston and M. S. Wu, *Foundation of Cellular Neurophysiology* (MIT Press, MA, 1999).
[5] C. Koch, *Biophysics of Computation* (Oxford University Press, Oxford, UK, 1999).
[6] T. H. Bullock and M. C. McClune, Electroencephalogr. Clin. Neurophysiol. **73**, 479 (1989).
[7] M. Steriade and F. Amzica, Proc. Natl. Acad. Sci. U.S.A. **93**, 2533 (1996).
[8] R. Eckhorn, R. Bauer, W. Jordan, M. Brosch, W. Kruse, M. Munk, and H. J. Reitboek, Biol. Cybern. **60**, 121 (1988).
[9] C. M. Gray, and W. Singer, Proc. Natl. Acad. Sci. U.S.A. **86**, 1698 (1989).
[10] A. Destexhe, D. Contreras, and M. Steriade, J. Neurosci. **19**, 4595 (1999).
[11] P. Acherman and A. A. Borbely, J. Neurosci. **85**, 1195 (1998).
[12] P. L. Nunez, *Neocortical Dynamics and Human EEG Rhythms* (Oxford University Press, New York, 1994).
[13] W. Rall and G. M. Shepherd, J. Neurophysiol. **31**, 884 (1968).
[14] M. Klee and W. Rall, J. Neurophysiol. **40**, 647 (1977).
[15] T. D. Lagerlund and F. W. Sharbrough, Comput. Biol. Med. **18**, 267 (1988).
[16] A. Destexhe, J. Neurosci. **18**, 9099 (1998).
[17] A. D. Protopapas, M. Vanier, and J. Bower, in *Methods in Neuronal Modeling* 2nd ed., edited by C. Koch and I. Segev (MIT Press, Cambridge, MA, 1998), pp. 461–498.
[18] C. Bédard, H. Kröger, and A. Destexhe, Biophys. J. **86**, 1829 (2004).
[19] V. Braitenberg and A. Schüz, *Cortex: Statistics and Geometry of Neuronal Connectivity*, 2nd ed. (Springer-Verlag, Berlin, 1998).
[20] A. Peters, S. L. Palay, and H. F. Webster, *The Fine Structure of the Nervous System* (Oxford University Press, Oxford, UK, 1991).
[21] S. Ramón y Cajal, *Histologie du Système Nerveux de l'Homme et des Vertébrés* (Maloine, Paris, 1909).
[22] J. B. Ranck, Exp. Neurol. **7**, 144 (1963).
[23] S. Orlowska, Doctoral thesis, Ecole Centrale, Lyon, France (unpublished).
[24] P. Debye and E. Hückel, Phys. Z. **24**, 185 (1923).